

MMFNet: A Multi-modality MRI Fusion Network for Segmentation of Nasopharyngeal Carcinoma

Huai Chen^a, Yuxiao Qi^a, Yong Yin^b, TengXiang Li^b, Guanzhong Gong^b,
Lisheng Wang^a,

^a*Institute of Image Processing and Pattern Recognition, Department of Automation,
Shanghai Jiao Tong University, Shanghai, 200240, P. R. China*

^b*Shandong Cancer Hospital Affiliated to Shandong University, Jinan, 250117, P.R. China*

Abstract

Segmentation of nasopharyngeal carcinoma (NPC) from Magnetic Resonance (MRI) Images is a crucial procedure for radiotherapy to improve clinical outcome and reduce radiation-associated toxicity. It is a time-consuming and label-intensive work for radiologists to manually mark the boundary of NPC slice by slice. In addition, due to the complex anatomical structure of NPC, automatic algorithms based on single-modality MRI do not have enough capability to get accurate delineation. To address the problem of weak distinction between normal adjacent tissues and lesion region in one single modality MRI, we propose a multi-modality MRI fusion network (MMFNet) to take advantage of three modalities MRI to realize NPC's segmentation. The backbone is a multi-encoder-based network, which is composed with several modality-specific encoders and one single decoder. The skip connection layer is utilized to combine low-level features from different modalities MRI with high-level features. Additionally, a fusion block is proposed to effectively fuse features from multi-modality MRI. Specifically speaking, the fusion block firstly highlight informative features and regions of interest, and then these weighted features will be fused and be further refined by a residual fusion block. Moreover, a training strategy named self-transfer is proposed to initializing encoders for

Email addresses: gongguanzhong@yeah.net (Guanzhong Gong), lswang@sjtu.edu.cn (Lisheng Wang)

multi-encoder-based network, it can stimulate encoders to make full mining of specific modality MRI. Our proposed framework can effectively make use of multi-modality medical datasets and the proposed modules such as fusion block and self-transfer can easily generalize to other multi-modality-based tasks.

Keywords: nasopharyngeal carcinoma, segmentation, multi-modality MRI, fusion block, self-transfer.

1. Introduction

Nasopharyngeal carcinoma (NPC), which has an unknown and complicated etiology, is a kind of malignant tumor. The distinctive geographic distribution of NPC makes some regions such as Southeast Asia, South China, the Arctic and the Middle East/North Africa have extremely higher incidence than other regions [1, 2]. And patients with early detection and diagnosis of NPC will have a greater 10-year survival rate, with 98% for stage I and 60% for stage II. On the contrary, the median survival of patients at advanced stage is only 3 years [3]. As a result, timely and effective treatment plays a crucial part in reducing the mortality of NPC. And radiotherapy, which highly depends on medical images such as the Magnetic Resonance (MRI) Images to get accurate delineation of the gross tumor volume (GTV), is the mainstay of treatment for NPC [4, 5, 6]. Moreover, in radiotherapy, accurate segmentation of NPC is necessary to separate normal adjacent tissues from lesion region to reduce radiation-associated toxicity [6]. Thus, before developing radiotherapy plans, clinicians need to manually mark the boundary of NPC slice by slice carefully. It is time-consuming and labor-intensive. Whats worse, the quality of segmentation highly depends on the experience of clinicians. Therefore, an automatic and precise segmentation approach is urgently needed to alleviate the workload of clinicians and improve efficacy of treatment presently.

Recently, according to the type of features used, methods of NPCs segmentation can be divided into two categories, one is based on traditional handcrafted features, while, the other is based on deep features obtained from deep neural

network (DNN). In traditional methods, besides relatively simple manmade features of medical images, such as intensity [7, 8, 9, 10], texture [11] and shape [12, 13], some traditional knowledge-based methods such as support vector machine (SVM) [14, 15, 16], semi-supervised fuzzy c-means [17, 11], dictionary learning [18] are also implemented to generate NPC’s boundary. Huang et al. [13] proposed a three-step NPC segmentation method in MRI. An adaptive algorithm was firstly performed to get the region of NPC due to similar localization of it in the head. Then, distance regularized level set was applied to determine the contour. Finally, the segmentation was further refined by a novel HMRF-EM framework based on the maximum entropy. Wang et al. [18] introduced a multi-modality-based method to take advantage of both CT and MRI to realize NPC’s contour. In this method, three dictionaries were learnt simultaneously based on joint dictionary learning using the information of training CT and MRI images patches and corresponding label. After getting dictionaries, the sparse coefficients for test volumes could be obtained by adopting sparse representation on these dictionaries. Finally, pixel-level label probability could be obtained by applying coefficients on the label dictionary learnt from joint dictionary learning.

Frameworks based on handcrafted features and traditional knowledge-based methods have been successfully implemented in the above papers to complete NPC segmentation in medical images. Nevertheless, the complex anatomical structure of NPC and the similarity of intensities between nearby tissues make it different to be accurately segment only with the help of manual features. Meanwhile, the high diversity of shapes and size makes this task more challenging [13]. Therefore, inspired by the success of deep learning technology, some methods [19, 20, 21, 22, 23] based on DNN were proposed to get more accurate segmentation in recent years. Ma et al. [19] developed an image-patch-based convolutional neural network (CNN) to combine CT and T1-weighted (T1W) images to realize NPC’s segmentation. In this method, two normal CNN-based classification networks were integrated into a Siamese-like sub-network. Therefore, both information from CT and MRI can be utilized with the assistance

of multi-modality similarity metric learning. Ma et al. [20] proposed a method combine CNN and graph cut. According to this framework, three CNN-based networks, which focus on axial, sagittal and coronal view respectively, were utilized to predict the probability of a voxel to be the tumor or non-tumor based on patches from three different views. Then, the initial segmentation, which is generated through intergrating results obtained from these three views, would be refined using a 3D graph cut-based methods.

Previous deep-learning-based work has established some excellent frameworks for NPC’s segmentation. Nevertheless, there remains the following deficiencies.

- (1) Although some DNN-based frameworks have been proposed recently to improve the performance of NPC’s segmentation [19, 20, 21, 22, 23], all of them are patch-based methods, which use a fixed-scale sliding window to crop image and determine the class of the center point. The performance of these frameworks highly depends on the size of sliding window and is dramatically time-consuming due to severe computing redundancy. What’s worse, all of above methods make predictions base on 2D slices of medical images, which ignore the vital role that 3D information plays in decision-making. Although Ma et al. [20] propose a method utilizing three-views, this framework still fails to make full use of three-dimensional information.
- (2) Currently, there is still no effort to fuse multiple modalities of MRI data to develop an automatic segmentation system for NPC. For delineation of NPC, MRI is the perferred imaging modality for its superior soft tissue contrast [24, 25, 6, 5]. Moreover, different modalities of MRI data have different visual characteristics and have various response to different tissues and anatomical structures. For example, T1-weighted (T1) MRI is suitable for detecting skull base involvement and fat planes, while contrast-enhanced T1-weighted (CET1) MRI is used to identity tumor extent [5]. Figure 1 shows some examples of NPC’s response in T1, CET1

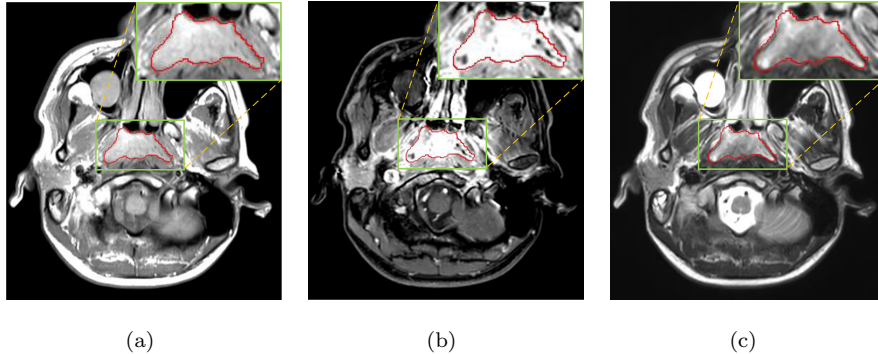


Figure 1: Examples of three multi-modality MRI (T1, CET1 and T2), the contour of NPC is marked in red line. (a),(b) and (c) are slices from T1 , CET1 and T2 respectively.

and T2-weighted (T2) MRI. Meanwhile, Popovtzer et al. [25] carried out a series of experiments to explore which sequences should be used for GTV delineation in planning radiotherapy. According to results of their work, it should be a routine clinical practice to incorporate all MRI datasets in highly conformal radiation therapy to realize GTV delineation. What's more, using multi-modality MRI data to generate the boundary of brain tumors like gliomas and glioblastomas is a generally accepted practice [26, 27, 28, 29].

In this paper, we focus on fusing multiple modalities MRI datasets to improve the performance of NPC segmentation. A end-to-end encoder-decoder network (MMFNet) with multi-modal encoders is proposed to combine three modalities MRI (T1, CET1, T2) to obtain segmentation of lesion. The skip connection utilized to combine low-level features and high-level features. Meanwhile, a fusion block is presented to effectively fuse features extracted respectively from three modalities MRI. In additional, we utilize a training strategy named self-transfer to stimulate encoder networks to make full mining features from different modalities data.

The main contributions of this paper can be summarized as followed:

- (1) To the best of our knowledge, we are the first one to propose a effec-

tive multi-encoder framework to utilize T1, CET1 and T2 MRI to realize NPC’s segmentation. According to our experiments, the usage of three modalities MRI can dramatically improve segmentation results.

- (2) A fusion block is presented to effectively fuse features extracted from different multiple-modality MRI to learn complementary features and cross-modal interdependencies.
- (3) A training strategy named self-transfer is utilized to enhance the capacity of features’ extracting for encoder networks.

The remaining paper is organized as followed. In section 2, related works will be reviewed. Section 3 will introduces our proposed framework, then experimental results and analysis will be reported in section 4. Finally, a conclusion will be made in section 5.

2. Related work

2.1. Deep learning technology

Since Hinton et al. [30] proposed an improved model to break through the bottleneck of deep learning, this technology has been rapidly developed. Several fields such as computer vision (CV), natural language processing (NLP), data mining, etc. have been considerably improved. Specially, in CV, great breakthroughs have been made in image classification [31, 32, 33, 34, 35], target recognition [36, 37, 38], sementic segmentation [39, 40, 41, 42, 43], etc.. Sementic segmentation plays a critical role in automatic drive, precision medicine, etc., and can be regarded as a task of pixel-by-pixel classification. In medical image processing, segmentation of target regions such as lesion [26, 44, 45], organs [46, 47] and cells [41] are important parts of computer-aided diagnosis and medical image visualization.

In initial DNN-based segmentation network [39, 40], pooling layers are utilized to expend receptive field to enable features to reflect global content information. While, the spatial resolution will decrease in the same time, which

will cause segmentation errors in tiny structures of objects. How to obtain a large enough receptive field to capture content features of targets and keep spatial resolution high enough to alleviate misjudgement of tiny structure is the vital challenge of segmentation network. Among all strategies proposed to solve this problem, both PSPNet [48] and DeepLab series [49, 43] are superior frameworks. PSPNet applies a pyramid parsing module to capture representations with different receptive fields, then, these features will be sampled up and concatenated to fuse local and global information. In DeepLab series network, atrous convolution is proposed to solve contradiction between requirement of high spatial resolution and large receptive field. Compared to normal convolutional layer, atrous convolution has special dilated kernel, which is inserted zeros in varies rates. Various dilated rate will make convolutional layer possess different receptive fields without increasing the size of kernel. Based on atrous convolution, Atrous Spatial Pyramid Pooling (ASPP) [49] and latest DenseASPP [43] present powerful capability of fusing features with various receptive fields without increasing parameters and decreasing spatial resolution.

Compared to PSPNet and models based on atrous convolution, both of which propose a novel architecture to increase receptive field without decrease spatial resolution, U-net [41] propose a skip connection framework to combine low-level and high-level features respectively produced from encoder and decoder to make final predictions. The encoder network captures high-level representation with stacking of convolutional layers and max-pooling layers, while, decoder network upsamples feature maps and map them to the final target modality. The use of skip connection layers to merge low-level features and high-level features has greatly improve the accuracy of segmentation and dramatically affected the subsequent methods. Therefore, the base architecture of our framework is similar to U-net, and skip connection layers are also utilized to connect encoder’s and decoder’s outputs.

2.2. Attention mechanism

In human perception, the information gained from different sensory channels will be weighted by attention mechanism, namely, greater weights will be ascribed to sensory streams providing reliable information from the world [50]. Specially, in human visual attention mechanism, only a subset of sensory information will be selected by intermediate and higher visual processes to be further processed [51]. The idea of attention mechanism has been successfully implemented in several frameworks of DNN for image classification [52, 53, 35, 54], image understanding [55, 56, 57], target detection [54], etc.. For attention mechanism, channel attention modules and spatial attention modules are two major topics. Channel attention modules attempts to adaptively recalibrate channel-wise feature responses. SENet [35] is a typical representation for channel-attention-based framework, which proposes a block named *Squeeze-and-Excitation* (SE) block to modelling interdependencies between channels and generate a series of coefficients to highlight informative features. Compared to channel attention modules, which focus on the importance of different features, spatial attention models emphasize the usage of concentrating on regions of interest. Wang et al. [53] presented Residual Attention Network to utilize soft weight mask generated by a soft mask branch to decide where features to attend. In addition to using one of these two modules separately, there also exist methods combining channel attention and spatial attention. CBAM [54] is a lightweight architecture simultaneously employs both spatial and channel-wise attention to improve performance of DNN. In this method, both max-pooling outputs and average-pooling outputs are extracted and fed into a shared multi-layer perceptron (MLP) to obtain channel-wise attention. Meanwhile, similar pooling outputs along channel axis are fed into a convolutional block to produce spatial attention.

Inspire by CBAM, we propose a fusion block to produce channel-wise attention and spatial attention for feature maps from three modalities MRI. Besides max-pooling outputs and average-pooling outputs, standard deviations (std) are also utilize to create channel-wise and spatial attention. Compared to CBAM,

which uses a shared multi-layer perceptron (MLP) to capture channel attention, the fusion block respectively set three MLPs for these three kinds of features.

2.3. Multi-modal fusion

Multi-modal fusion is widely used in CV for semantic segmentation [58, 59, 60], classification [61, 62], image fusion [63, 64, 65] and image registration [66, 67]. Multi-modal images such as RGB-D [58, 59] and thermal streams [68] are utilized in natural images. Specially, in medical images, combining multi-modality images such as CT, T1 MRI, T2 MRI, etc. to realize multi-organ segmentation [47] and lesion segmentation [26, 27] is widely adopted due to distinct responses of different modalities for different tissues. Tseng et al. [26] presented a novel framework to combine four modalities MRI to complete brain tumor segmentation. Feature maps of slices from multiple modalities MRI are firstly extracted through putting them into multi-modal encoders. Then, a cross-modality convolution block is proposed to fuse feature maps of different modalities data. And convolutional LSTM is utilized as a key block to explore correlations between consecutive slices. It is a representative method of multi-modal encoders, which use multiple modality-specific network to extract feature maps at various levels. Compared to intuitive early fusion technique [69], which stack multi-modality images channel-wise and feed them to a single encoder, methods based on multi-modality encoders have better capability to capture complementary features [70].

Due to the superiority of multi-modal encoders, we use three modality-specific encoders to capture representations of three modalities MRI. Then, we propose fusion block to fuse three kinds of representations. Finally, a decoder merge fused features and features upsampled by decoder to make final predictions.

3. Methodology

As illustrated in figure 2, our framework is an end-to-end fully convolutional network, which contains three encoder networks to take three volume blocks

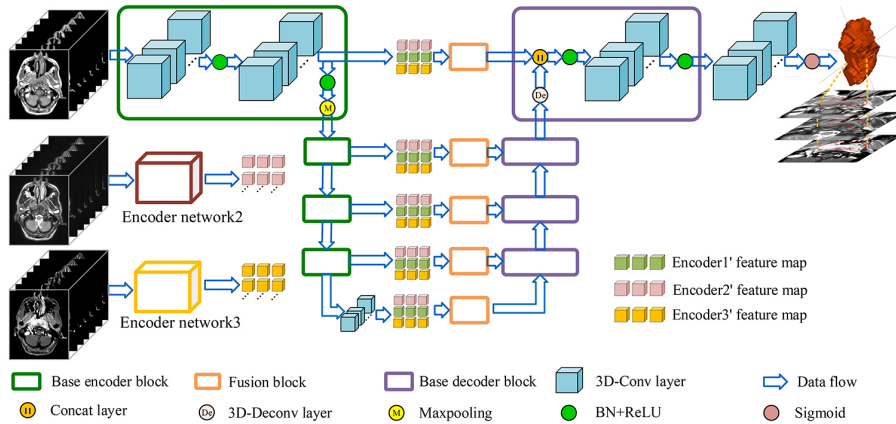


Figure 2: An illustration of our proposed framework.

of three modalities MRI as input. The encoder network is a VGG-like [31] DNN, which stacks base block containing several convolution layers followed by a max-pooling layer to get deeper features. While, the decoder network use deconvolutional layers to upsample feature maps, the final output is a feature map with the same scale as input. A fusion block is proposed to fuse feature maps from different encoders, and the fused low-level features are merged with features produced by deconvolutional layer to realize the combination of low-level features and high-level features. For the training of network, we propose self-transfer to use pre-trained modality-specific encoders, which is trained with one single modality, as initial encoders of multi-modality model. The use of self-transfer can effectively improve the performance of encoders and make full mining of informative features of each modality data.

3.1. Base encoder-decoder network

Inspired by U-net [41], our base encoder-decoder can be seen as a U-net composed with 3D convolutional layers and deconvolutional layers. Through stacking convolutional layers and max-pooling layers, encoder network can get larger receptive field, meanwhile, the spatial resolution becomes smaller. On the contrary, decoder network is composed with deconvolutional layers to upsample

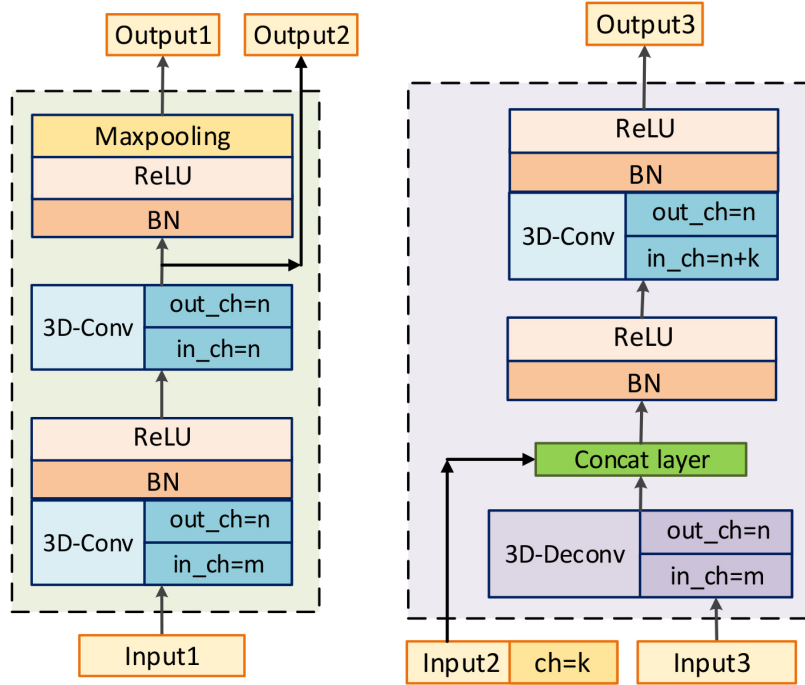


Figure 3: An illustration of base encoder block and base decoder block. Left: base encoder block. Right: base decoder block. Input1, Input3: feature maps from previous block. Input2: feature maps produced by corresponding encoder block with the same spatial scale as output of 3D-Deconv layer. Output1, Output3: feature maps, which will be fed into next block. Output2: feature maps, which will be fed into the corresponding decoder block through skip connection layer.

feature maps, thus, the spatial resolution of features can recover to original scale when high-level features go through decoder. As described in [71], higher layers capture the high-level content representation, while, lower layers capture style representation such as texture. And for semantic segmentation, both content and style representations should be utilized, so skip connection layers is adopted to combine low-level features and high-level features with the same spatial resolution. The architectures of base encoder block and decoder block are illustrated in figure 3.

Base encoder network. Our encoder network is a VGG-liked [31] network,

and the base block is composed with two 3D convolutional layers. According to [72], the representation size should slightly decrease to avoid bottlenecks with enormous compression. Therefore, the $3 \times 3 \times 3$ 3D-convolutional layers and $2 \times 2 \times 2$ max-pooling layers are preferential choices to compose our network. A encoder block is composed with two convolutional layers. And after convolution, a batch normalization layer and ReLU layer are followed. There are two outputs produced by encoder block, one is for next encoder block, the other is for the corresponding decoder block to realize the combination of both high-level and low-level feature maps. There are totally four encoder blocks and the channel of output (*Out_ch*) are 8, 16, 32 and 64 respectively. And it is worth mentioning that there is one single convolutional layer after final encoder block to refine features downsampled by encoder block, and the number of its channels is 64.

Base ecoder network. The purpose of decoder network is to map high-level features to target modality. A 3D-deconvolotional layer is utilized to up-sample feature maps, then, a concatenation layer combine these features with features from encoders with the assistance of skip connection architecture. After merging, a convolutional layer is adopted to fuse these feature maps. The output’s channel of decoder are 64, 32, 16 and 8 respectively.

Finally, the final decoder block is followed by a convolutional layer with sigmoid as activation to produce final segmentation results.

Loss function. Inspired by [46], which present Dice coefficient to effectively solve imbalance in the number of voxels of foreground and background, we apply Dice loss as network’ optimization objective. We denote ground truth as G and P is denoted as predict results. The definition of Dice loss is shown as:

$$Loss_{dice} = 1 - 2 \times \frac{\sum_{i=1}^N p_i g_i + \epsilon}{\sum_{i=1}^N p_i + \sum_{i=1}^N g_i + \epsilon} \quad (1)$$

$$p_i \in P \quad (2)$$

$$g_i \in G \quad (3)$$

Where ϵ is smoothness term to avoid the risk of devision by 0, and we set $\epsilon = 1$ in our experiments.

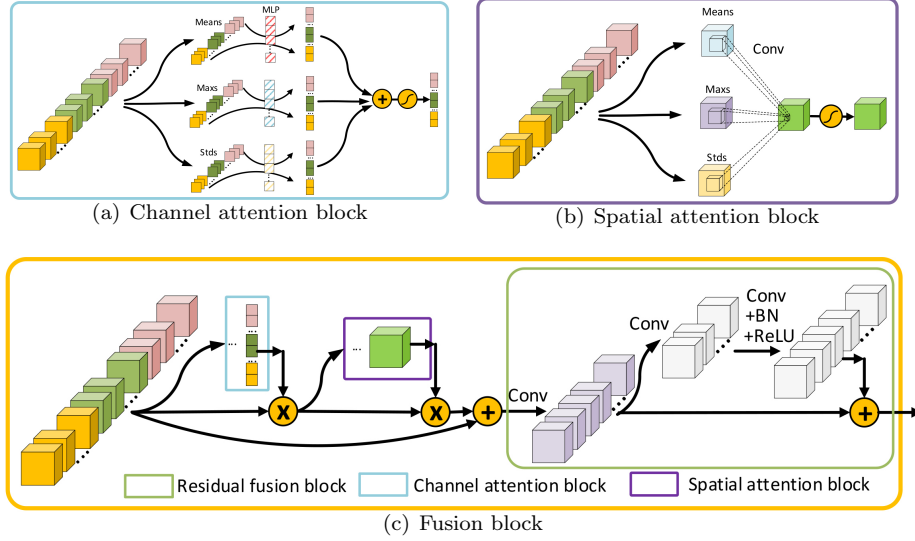


Figure 4: The architecture of channel attention block, spatial attention block and fusion block.

3.2. Fusion block

The fusion block is composed with a channel attention block, which focuses on 'what' are meaningful features, a spatial attention block, which focuses on where is an interesting part, and a residual fusion block, which fuses weighted feature maps and refines them. We concatenate feature maps from three encoders and feed them into the fusion block to produce fused ones, followed that, the fused features will be combined with high-level features through skip connection layers. The architectures of channel attention block, spatial attention block, residual fusion block and fusion block are shown in figure 4.

Given three intermediate feature maps from multiple encoders $F_1, F_2, F_3 \in R^{C \times D \times H \times W}$ as inputs. We firstly merge them on channel axis to obtain total original feature maps $F_{ori} \in R^{3C \times D \times H \times W}$. And we denote the final fused features as F_{fused} , the overall fusing process can be summarized as followed:

$$F_c = W_c(F_{ori}) \otimes F_{ori} \quad (4)$$

$$F_s = W_s(F_c) \otimes F_c \quad (5)$$

$$F_{fused} = Res(F_s + F_{ori}) \quad (6)$$

We denote \otimes as element-wise multiplication, which will automatically broadcasts spatial attention weights (W_s) and channel attention weights (W_c) to fit input feature maps. Meanwhile, F_c and F_s are denoted as feature maps after being refined by channel attention block and spatial attention block respectively. F_{fused} is the final output, which is fused and refined by residual fusion block.

Channel attention block. The focus of channel attention block is to selectively emphasize feature maps, which are meaningful for final predictions. SENet [35] utilizes global average pooling to capture average-values of each feature map, and feed them into a MLP to get weights for every channel. Compared to SENet, the channel attention block of CBAM [54] uses global max-pooling layers to get max-values of feature maps in addition to capturing average-values using global average-pooling layers. In the same time, two vectors of average-values and max-values are fed into a shared MLP and output vectors are combined by add operation. In this paper, in order to better represent the global features for three-dimension feature maps, we capture stds of every three-dimension features and combine them with average-values and max-values to produce weights for every channel feature. We denote obtained stds, average-values and max-values as $F_{std}, F_{avg}, F_{max} \in R^{3c \times 1 \times 1 \times 1}$. In terms of MLP, we respectively set three MLPs for stds, average-values, max-values. All of these MLPs are composed with one hidden layer setting hidden activation size as $R^{3c/r \times 1 \times 1 \times 1}$, where r is the reduction ratio and we set $r = 12$ in our experiments. And the final output channel weights W_c has $3c$ values for each channel feature. The formulation for W_c is shown as followed:

$$W_c(F_{ori}) = \sigma(MLP_{avg}(F_{avg}) + MLP_{max}(F_{max}) + MLP_{std}(F_{std})) \quad (7)$$

$$F_{avg} = AvgPool(F_{ori}) \quad (8)$$

$$F_{max} = MaxPool(F_{ori}) \quad (9)$$

$$F_{std} = StdPool(F_{ori}) = (AvgPool((F - AvgPool(F_{ori}))^2))^{1/2} \quad (10)$$

Where σ is the sigmoid activation to produce channel-wise weights varied from 0 to 1. Figure 4(a) shows the architecture of channel attention block.

Spatial attention block. The purpose of spatial attention block is to utilize feature maps after channel-wise refining to obtain 3D spatial attention map (W_s). On the basis of previous work of CBAM, we capture stds, average-values and max-values along the channel axis and concatenate them to generate three 3D feature blocks. And these features are fed into a $3 \times 3 \times 3$ 3D convolutional layer with sigmoid as activation to produce W_s . Through element-wise multiplication, informative regions will be effectively highlighted. The architecture of spatial attention block is shown in figure 4(b), and the process can be summarized as followed:

$$W_s = \sigma(f^{3 \times 3 \times 3}([AvgPool(F_c); MaxPool(F_c); StdPool(F_c)])) \quad (11)$$

Where $f^{3 \times 3 \times 3}$ is denoted as one single convolutional layer with $3 \times 3 \times 3$ kernel size and the output channel is 1.

Residual fusion block. After highlighting informative features and regions, a residual fusion block is constructed to fuse and refine features. It is worth mentioning that the number of channels is $3c$ for $(F_{ori} + F_s)$, while, the corresponding high-level features, which is prepared to combine with fused features, only has c channels. Therefore, in order to keep balance between low-level and high-level features, a $1 \times 1 \times 1$ convolutional layer with c channel outputs is utilized to fuse feature maps and reduce channel’s number firstly. Then, a residual block is adopted to refine feature maps. This block is composed with two convolutional layers, both of them have $1 \times 3 \times 3$ kernels and the first one is followed by batch normalization layer and ReLU layer. We can summary this process using following equations:

$$F_r = f^{1 \times 1 \times 1}(F_{ori} + F_s) \quad (12)$$

$$F_{fused} = F_r + f^{1 \times 3 \times 3}(f^{1 \times 3 \times 3*}(F_r)) \quad (13)$$

Where F_r is feature maps after $1 \times 1 \times 1$ convolutional layer, and $f^{1 \times 3 \times 3*}$ is denoted as $1 \times 3 \times 3$ convolutional layer followed by batch normalization layer and ReLU.

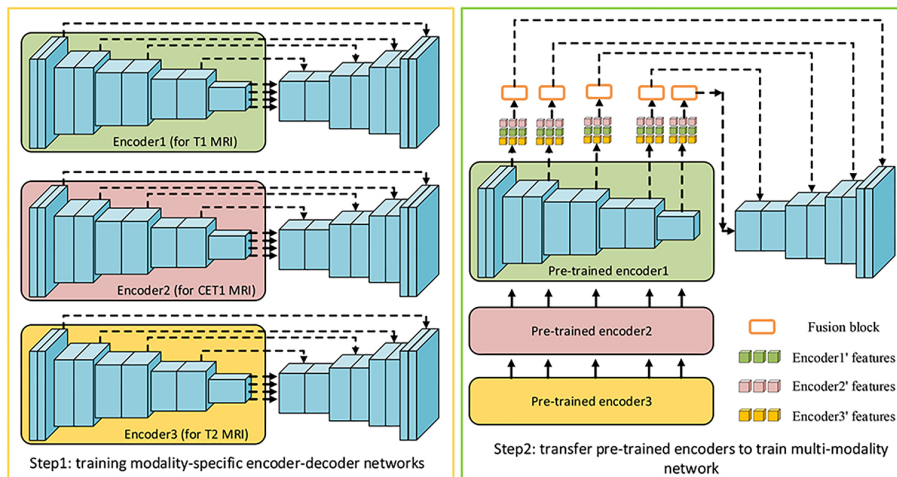


Figure 5: An illustration of the self-transfer learning.

3.3. Self-transfer learning

Transfer learning [73] is a popular trick to improve performance of systems. The use of a powerful pre-trained network as features' extractor can bring dramatical improvements to new systems. Hence, transfer learning is a preferred technique for several CV tasks [37, 36, 43]. And using a network pre-trained in imagenet as an encoder for a segmentation network is a common operation in natural images [43, 48, 39]. However, there is not a powerful enough 3D pre-trained model can be set as the initial features' extractor for various 3D medical images due to its complexity and various imaging technologies. Especially for multi-modality MRI, images of each modality have their own specific imaging styles, it's hard to obtain a feature extractor can be generalized to all of them. Therefore, we propose an initialization trick named self-transfer to transfer encoders of modality-specific models to multi-modality model. According to experimental results, performance of multi-modality model can obtain considerable improvements by using self-transfer.

Specifically speaking, a modality-specific model can effectively capture individual informative features from this modality data, while, a multi-modality model aims to obtain interdependent and complementary information from mul-

tiple modalities datasets. As a result, some individual features of one single modality may be ignored in multi-modality model. Therefore, we propose self-transfer to fully mine modality-specific features. Figure 5 is the illustration of self-transfer. The first step is to train three modality-specific encoder-decoder models. Then, these encoders will be used as the initial encoders for multi-modality model. Compared to original encoders with random initialization, these encoders have greater power to make full mining of individual features for specific modalities. Meanwhile, the fusion block and decoder can effectively fuse these features to obtain informative features for final predictions. We will set several experiments to demonstrate self-transfer can enhance the segmentation systems in the following paper.

4. Experiments and analysis

4.1. Dataset and Preprocessing

Dataset. Three modalities MRI of T1, CET1 and T2 of 149 patients are acquired at Shandong Cancer Hospital Affiliated to Shandong University hospital. The patients are scanned with Philips Ingenia 3.0T MRI system. Both CET1 and T2 are aligned to T1. After registering, we will resample XYZ spacing. Due to the spacings of X axis and Y axis are varied from $0.33mm$ to $0.69mm$, while, the spacing of Z axis ranges from $3.5mm$ to $5.5mm$, we resample the XY spacing to $0.5 \times 0.5mm^2$, while keep the spacing of Z fixed to avoid obtaining unreal images due to the large value of original spacing. The ground truth is created by an experienced radiologist and it is marked slice by slice.

Preprocessing. The preprocessing mainly contains intensity normalization and regions of interest (ROIs) cropping. Due to different imaging configurations of MRI, we utilize the intra-body intensity normalization proposed in [45], which effectively deals with the differences caused by imaging configurations and reduce the influence of inconsistent body-to-background ratios. We denote $X = (x_1, x_2, \dots, x_i)$ as the total original MRI data and x_i is one single MRI instance. We firstly use OTSU [74] thresholding to capture body mask m_i for x_i .

After obtain foreground, we calculate foreground’s mean and std, then subtract the mean from MRI data and devide it by std. The process can be summarized as followed.

$$mean_i = sum(m_i \times x_i) / sum(m_i) \quad (14)$$

$$std_i = [sum(m_i \times (x_i - mean_i)^2) / sum(m_i)]^{1/2} \quad (15)$$

$$x'_i = (x_i - mean_i) / std_i \quad (16)$$

Where x'_i is a MRI instance after normalization and we denote $X' = (x'_1, x'_2, \dots, x'_i)$ as the total MRI after normalization. After normalization, according to distribution histogram of normalized data , we clip (limit) values to reduce data complexity. Specifically speaking, through statistical analysis for values in NPC regions, we set a max value and min value to limit values. In this paper, we set $[-2, 1]$, $[-3, 2]$ and $[-2, 3.5]$ for T1, T2 and CET1 respectively.

Due to the similar location of NPC regions and the size of MRI is varied, we using sliding windows to crop regions with interest (ROIs) and feed them into network. Specifically speaking, we firstly using OTSU to get the 3D bounding box (3D-bbox) of original MRI and then we crop a $16 \times 256 \times 256$ region according to the center point of 3D-bbox. The sliding window slides on the Z axis and the sliding-step is 4, in addition, we perform on-the-fly data augmentation to apply random center offset from $(-4, -32, -32)$ to $(4, 32, 32)$, random vertical flipping and random rotation on the XY plane from -5° to 5° . The illustration of preprocessing is shown in figure 6

4.2. Evaluation metrics

1) *Dice Similarity Coefficient (DSC)*: The dice similarity coefficient is designed to evaluate the overlap rate of predict results and ground truth. DSC can be written as:

$$DSC(P, G) = \frac{2 \times |P \cap G|}{|P| + |G|} \quad (17)$$

DSC ranges from 0 to 1, and the better prediction will have larger DSC.

2) *Average Precision (AP)*: It is the average precision score at different recall scores. We use different thresholding values to classify pixels into background

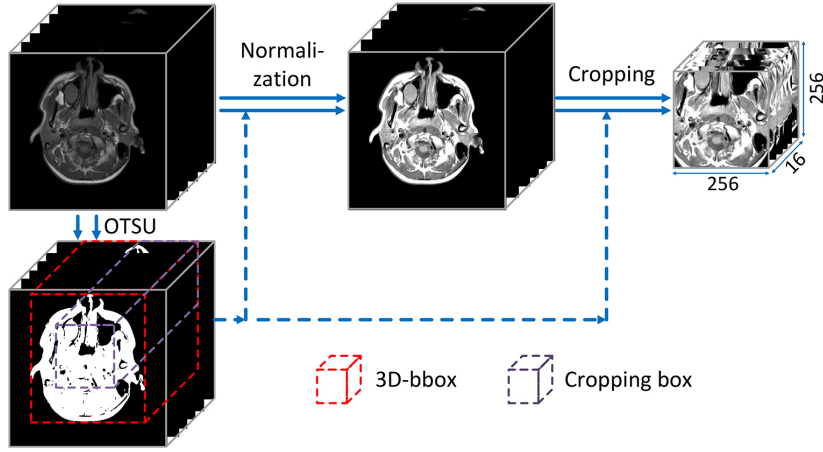


Figure 6: An illustration of preprocessing.

or foreground and get several pairs of recall values and precision values. The definition of AP is shown as followed.

$$AP = \int_{recall=0}^{recall=1} precision \quad (18)$$

$$recall = \frac{TP}{TP + FN} \quad (19)$$

$$precision = \frac{TP}{TP + FP} \quad (20)$$

Where TP is the number of true positives, FP is the number of false positives and FN is the number of false negatives.

4.3. Implementation details

The architectures of base encoder, base decoder and fusion block are described in detail in section 3.1 and 3.2. We set extensive experiments to present the improvements brought by the utilization of multi modalities MRI and the novel multi-modal fusion network proposed. For the evaluation metric of DSC , we set the thresholding value as 0.5.

Combination of multi-modality MRI. In this part, we aim to demonstrate that using multi-encoder-based network to combine all T1, CET1 and T2 MRI images will obtain more precise delineations for NPC. We firstly set

three modality-specific encoder-decoder networks for T1, T2 and CET1. The design for modality-specific network is a combination of base encoder network and base decoder network described in section 3.1, skip connection layers are utilized to merge corresponding low-level and high-level features. And we feed single modality MRI images to train the network. Then, we try two mainstream multi-modality framework. The first one is single-encoder-based network, which stack different modalities images channel-wise and fed them into a single encoder and a single decoder. The other one is multi-encoder-based network, which provides specific encoders for different modalities images. For the multi-encoder-based network, the architecture of encoders are all base encoder networks aforementioned. While for the encoder of single-encoder-based network, we set the number of encoder’ channel to be three times of base encoder in order to keep single-encoder-based network and multi-encoder-based network have the same number of encoder’s features, that is to say, the encoder’ channel number for single-encoder-based network is 24, 48, 96 and 192 respectively.

The utilization of fusion block. We set several ablation experiments to show the improvements brought by the utilization of fusion block. Firstly, the original MMFN is composed with a base fusion block and base multi-modality network, and the base fusion block is made up of residual fusion block and stacking 3D-CBAM, which utilizes max-pooling outputs and average-pooling outputs to get channel attention and spatial attention. Secondly, we replace the shared MLP in channel attention block with several independent MLPs. Then, std-pooling outputs are respectively utilized in channel attention block and spatial attention block. Finally, the outputs of std-pooling are implemented to combine with original max-pooling outputs and average-pooling outputs to form channel attention block and spatial attention block.

The contribution of self-transfer. After setting several experiments to add different fusion blocks to multi-modality network, we implement self-transfer to these models to investigate efficacies of using it. The pre-trained features’ extractors are encoders aforementioned, which are implemented to analyze the efficacy of utilization of multi-modality MRI.

All above methods are evaluated in five-fold cross validation. And 25% of training data will be divided as validation data to choose best model and avoid overfitting. For the training of above networks without self-transfer, we use Adam [75] as optimizer at a learning rate of 10^{-3} . For the training of self-transfer-based methods, we will firstly train three modality-specific networks, then, transfer pre-trained encoders as initialization features' extractors for multi-modality network. For the first 5 training epochs of these networks, we keep encoders fixed and set Adam with learning rate of 10^{-3} to warm-up decoder, and encoders will be fine-tuned with learning rate of 10^{-4} after warming up. For all above networks, we set batch-size as 8 and each epoch will update network 75 times. In the same time, we use early-stopping strategy to stop training if validation loss does not decrease over 10 epochs to reduce overfitting. The max epoch is 100.

Our experiments are performed on a workstation platform with Intel(R) Xeon(R) CPU E5-2620 v4 @ 2.10GHz, 64GB RAM and 2x NVIDIA Titan Xp GPU with 12GB GPU memory. The code is implemented with pytorch 0.4.1 in Windows 10.

4.4. Results

Table 1 reports the values of DSC , AP and $Loss_{dice}$ for different methods. The predicted masks of different methods are illustrated in figure 7 and figure 8, which respectively present results in 2D and 3D images. We comprehensively analyze this data and draw following conclusions.

Firstly, through comparing modality-specific networks, single-encoder multi-modality network and multi-encoder multi-modality network, we demonstrate that the utilization of multi-modality MRI and multi-encoder network can significantly improve the performance of NPC' segmentation. It can respectively bring 3.74%, 5.19% and 0.045 improvements in DSC , AP , $Loss_{dice}$ compared to the best modality-specific network, which only utilize T1 MRI to realize segmentation. Different modality MRI have various response to different tissues and anatomical structures. Therefore, the utilization of multi-modality MRI

Table 1: Comparison of NPC segmentation results using different methods.

Method	<i>DSC</i>	<i>AP</i>	<i>Loss_{dice}</i>
Modality-specific network (T1)	0.6817	0.7202	0.3361
Modality-specific network (T2)	0.6589	0.6920	0.3610
Modality-specific network (CET1)	0.6222	0.6456	0.3921
Single-encoder multi-modality network	0.6552	0.6954	0.3556
Multi-encoder multi-modality network (baseline)	0.7005	0.7439	0.3141
MMFN	0.7007	0.7494	0.3129
MMFN + multi-MLP	0.7083	0.7508	0.3046
MMFN + multi-MLP +stdPool (channel-attention)	0.7095	0.7602	0.3015
MMFN + multi-MLP +stdPool (spatial-attention)	0.7010	0.7482	0.3123
MMFN + multi-MLP +stdPool (channel-attention & spatial-attention)	0.7189	0.7648	0.2938
MMFN + self-transfer	0.7095	0.7589	0.3018
MMFN + multi-MLP + self-transfer	0.7128	0.7659	0.2971
MMFN + multi-MLP +stdPool + self-transfer	0.7191	0.7721	0.2907

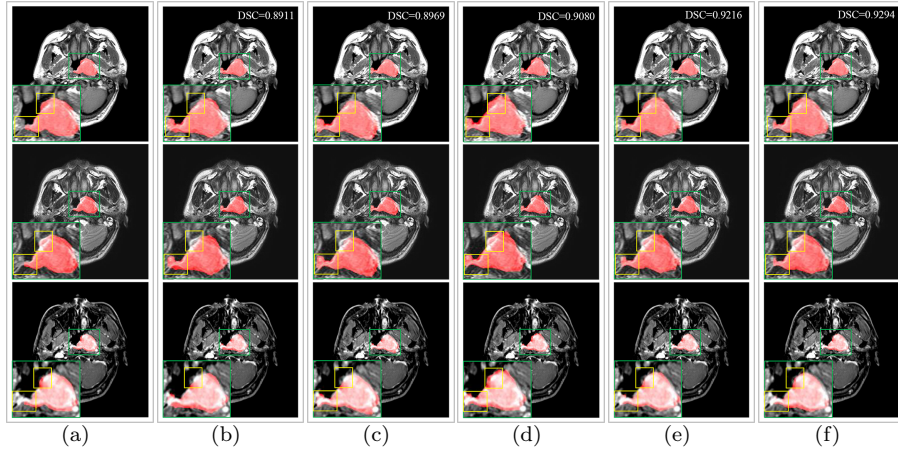


Figure 7: Predicted results in one single slice image, there are corresponding T1, T2 and CET1 images from top to down. And the DSC value is the dice similarity coefficient of this single slice. (a) Ground truth. (b) Predicted region of modality-specific network (T1). (c) Predicted region of single-encoder multi-modality network. (d) Predicted region of multi-encoder multi-modality network. (e) Predicted region of MMFN + multi-MLP + stdPool. (f) Predicted region of MMFN + multi-MLP + stdPool + self-transfer.

can make network to learn complementary and interdependent features for final decisions. Multi-encoder network, which is composed with several specific encoders for different modalities MRI and one single decoder, can effectively capture informative features from different datasets and fuse all low-level features and high-level features. While, compared to multi-encoder-based network, single-encoder-based network cannot perform well due to the extremely large differences among different modalities MRI, which makes directly capturing features from stacking data is confusing for encoder.

Next, the design of fusion block can successfully fuse features from different modality-specific encoders and bring improvements for multi-modality segmentation network. The fusion block contains a channel attention block and spatial attention block to highlight informative features and regions of interest. Compared to original CBAM, which uses a shared MLP to combine max-pooling outputs and average-pooling outputs get channel attention, fusion block proposed in this paper utilizes specific MLPs for different categories of features

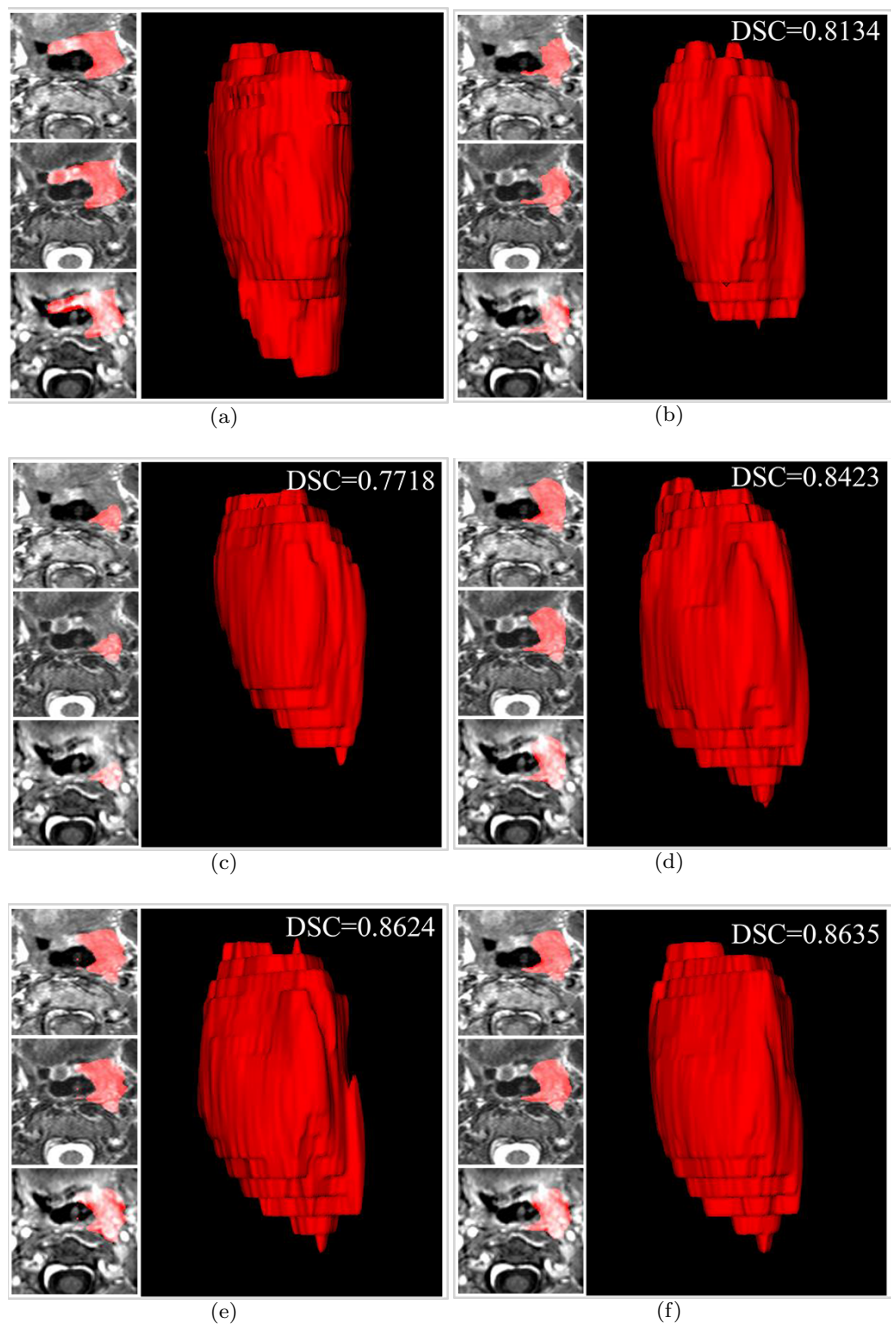


Figure 8: Examples of 3D predicted results for different methods. (a) Ground truth. (b) Predicted region of modality-specific network (T1). (c) Predicted region of single-encoder multi-modality network. (d) Predicted region of multi-encoder multi-modality network. (e) Predicted region of MMFN + multi-MLP + stdPool. (f) Predicted region of MMFN + multi-MLP + stdPool +self-transfer.

and add std-pooling outputs to provide more adequate global information. And according to experimental results, the addition of stds is meaningful to spatial attention block. In addition, we respectively add std-pooling to channel attention block, spatial attention block and both of them, the results shows that the utilization of std-pooling both in channel attention block and spatial attention block can achieve best result. Therefore, we recommend that both channel attention block and spatial attention block should utilize std-pooling outputs.

Additionally, we set three experiments to show the effectiveness of self-transfer. The using of self-transfer can improve the performance of networks compared to original networks. Self-transfer, which use pre-trained modality-specific encoders as the initial encoders for multi-encoder network, can make full mining of informative features for specific modality data. Additionally, self-transfer is a great strategy for segmentation network of 3D multi-modality medical images, which cannot find an enough powerful 3D network as initial features' extractor due to the complexity of imaging, to make an excellent initialization for feature extractors.

Finally, our proposed network is extremely time-friendly compared to manually marking by radiologists, specifically speaking, our proposed method only needs about 9s to realize NPC's delineation of a patient, while, an experienced radiologist needs 10 to 20 minutes to realize it. In addition, through analyzing the 3D mask of proposed method and man-made label, the result of our method is state-of-the-art and even smoother than manual label due to the utilization of 3D image blocks as inputs, which enable the network captures information from a series of slices and get smoother and more continuous contours.

5. Conclusion

In this paper, we propose a novel multi-modality MRI fusion network (MMFNet) for segmentation of nasopharyngeal carcinoma (NPC). We emphasize the importance of utilizing multi-modality MRI to realize accurate NPC's delineation. In the same time, we discuss two existing mainstream frameworks for multi-

modality datasets, one is single-encoder-based network, which stacks different multi-modality data channel-wise and feed them into a single encoder, the other one is multi-encoder-based network, which utilizes modality-specific encoders for different modalities data. According to experimental results, we draw a conclusion that multi-encoder-based methods are more powerful than single-encoder-based methods because simply stack multi-modality MRI with wide differences may confuse the features' extractor. Moreover, we propose a fusion block to effectively fuse features from different modalities. Inspired by attention mechanism, we design the fusion block with channel attention block, spatial attention block and a residual fusion block. In order to capture attention weights, we combine max-pooling outputs, average-pooling outputs and std-pooling outputs to represent global information for images and get weights mask according to these features. Additionally, we propose a training strategy named self-transfer to effectively initializing encoders of multi-encoder-based network. It is an extremely excellent strategy for features' extractor's initialization for multi-modality medical images. In principle, the proposed multi-modality MRI fusion network is a novel framework for multi-modality-MRI-based segmentation, and the proposed fusion block and self-transfer are effective and can easily generalize to other multi-modality-based tasks.

In the future, we will further improve our proposed method and generalize to other multi-modality-based tasks to lighten workload of clinicians. In addition, our method will be utilized as the preprocessing for Radiomics analysis in NPC.

References

References

- [1] E. T. Chang, H.-O. Adami, The enigmatic epidemiology of nasopharyngeal carcinoma, *Cancer Epidemiology and Prevention Biomarkers* 15 (10) (2006) 1765–1777.
- [2] M. A. Mohammed, M. K. A. Ghani, R. I. Hamed, D. A. Ibrahim, Review on nasopharyngeal carcinoma: Concepts, methods of analysis, segmentation,

- classification, prediction and impact: A review of the research literature, *Journal of Computational Science* 21 (2017) 283–298.
- [3] L. Wu, C. Li, L. Pan, Nasopharyngeal carcinoma: A review of current updates, *Experimental and therapeutic medicine* 15 (4) (2018) 3687–3692.
- [4] A.-C. Feng, M.-C. Wu, S. Y. Tsai, K.-Y. Chan, S. H. Cheng, A. Wang, S.-S. Chen, J. J. Jian, S.-D. Terng, A. T. Huang, Prevertebral muscle involvement in nasopharyngeal carcinoma, *International Journal of Radiation Oncology* Biology* Physics* 65 (4) (2006) 1026–1035.
- [5] A. A. K. A. Razek, A. King, Mri and ct of nasopharyngeal carcinoma, *American Journal of Roentgenology* 198 (1) (2012) 11–18.
- [6] C. M. Glastonbury, Nasopharyngeal carcinoma: the role of magnetic resonance imaging in diagnosis, staging, treatment, and follow-up, *Topics in Magnetic Resonance Imaging* 18 (4) (2007) 225–235.
- [7] F. K. Lee, D. K. Yeung, A. D. King, S. Leung, A. Ahuja, Segmentation of nasopharyngeal carcinoma (npc) lesions in mr images, *International Journal of Radiation Oncology* Biology* Physics* 61 (2) (2005) 608–620.
- [8] W. Chanapai, P. Ritthipravat, Adaptive thresholding based on som technique for semi-automatic npc image segmentation, in: *Machine Learning and Applications, 2009. ICMLA'09. International Conference on*, IEEE, 2009, pp. 504–508.
- [9] C. Tatanun, P. Ritthipravat, T. Bhongmakapat, L. Tuntiyatorn, Automatic segmentation of nasopharyngeal carcinoma from ct images: region growing based technique, in: *Signal Processing Systems (ICSPS), 2010 2nd International Conference on*, Vol. 2, IEEE, 2010, pp. V2–537.
- [10] W. Chanapai, T. Bhongmakapat, L. Tuntiyatorn, P. Ritthipravat, Nasopharyngeal carcinoma segmentation using a region growing technique, *International journal of computer assisted radiology and surgery* 7 (3) (2012) 413–422.

- [11] J. Zhou, T.-K. Lim, V. Chong, J. Huang, A texture combined multispectral magnetic resonance imaging segmentation for nasopharyngeal carcinoma, *Optical review* 10 (5) (2003) 405–410.
- [12] I. Fitton, S. Cornelissen, J. C. Duppen, R. Steenbakkers, S. Peeters, F. Hoebbers, J. H. Kaanders, P. Nowak, C. R. Rasch, M. van Herk, Semi-automatic delineation using weighted ct-mri registered images for radiotherapy of nasopharyngeal cancer, *Medical physics* 38 (8) (2011) 4662–4666.
- [13] K.-W. Huang, Z.-Y. Zhao, Q. Gong, J. Zha, L. Chen, R. Yang, Nasopharyngeal carcinoma segmentation via hmrf-em with maximum entropy, in: *Engineering in Medicine and Biology Society (EMBC), 2015 37th Annual International Conference of the IEEE, IEEE, 2015*, pp. 2968–2972.
- [14] J. Zhou, K. L. Chan, P. Xu, V. F. Chong, Nasopharyngeal carcinoma lesion segmentation from mr images by support vector machine, in: *Biomedical Imaging: Nano to Macro, 2006. 3rd IEEE International Symposium on, IEEE, 2006*, pp. 1364–1367.
- [15] J. Zhou, Q. Tian, V. Chong, W. Xiong, W. Huang, Z. Wang, Segmentation of skull base tumors from mri using a hybrid support vector machine-based method, in: *International Workshop on Machine Learning in Medical Imaging, Springer, 2011*, pp. 134–141.
- [16] W. Huang, K. L. Chan, J. Zhou, Region-based nasopharyngeal carcinoma lesion segmentation from mri using clustering-and classification-based methods with learning, *Journal of digital imaging* 26 (3) (2013) 472–482.
- [17] J. Zhou, V. Chong, T.-K. Lim, J. Houng, Mri tumor segmentation for nasopharyngeal carcinoma using knowledge-based fuzzy clustering, *International journal of information technology* 8 (2).
- [18] Y. Wang, B. Yu, L. Wang, C. Zu, Y. Luo, X. Wu, Z. Yang, J. Zhou, L. Zhou, Tumor segmentation via multi-modality joint dictionary learn-

- ing, in: Biomedical Imaging (ISBI 2018), 2018 IEEE 15th International Symposium on, IEEE, 2018, pp. 1336–1339.
- [19] Z. Ma, X. Wu, S. Sun, C. Xia, Z. Yang, S. Li, J. Zhou, A discriminative learning based approach for automated nasopharyngeal carcinoma segmentation leveraging multi-modality similarity metric learning, in: Biomedical Imaging (ISBI 2018), 2018 IEEE 15th International Symposium on, IEEE, 2018, pp. 813–816.
- [20] Z. Ma, X. Wu, Q. Song, Y. Luo, Y. Wang, J. Zhou, Automated nasopharyngeal carcinoma segmentation in magnetic resonance images by combination of convolutional neural networks and graph cut, *Experimental and therapeutic medicine* 16 (3) (2018) 2511–2521.
- [21] Y. Wang, C. Zu, G. Hu, Y. Luo, Z. Ma, K. He, X. Wu, J. Zhou, Automatic tumor segmentation with deep convolutional neural networks for radiotherapy applications, *Neural Processing Letters* (2018) 1–12.
- [22] Z. Ma, X. Wu, J. Zhou, Automatic nasopharyngeal carcinoma segmentation in mr images with convolutional neural networks, in: *the Frontiers and Advances in Data Science (FADS)*, 2017 International Conference on, IEEE, 2017, pp. 147–150.
- [23] A. Feng, Z. Chen, X. Wu, Z. Ma, From convolutional to recurrent: Case study in nasopharyngeal carcinoma segmentation, in: *the Frontiers and Advances in Data Science (FADS)*, 2017 International Conference on, IEEE, 2017, pp. 18–22.
- [24] J. Goh, K. Lim, Imaging of nasopharyngeal carcinoma, *Ann Acad Med Singapore* 38 (9) (2009) 809–16.
- [25] A. Popovtzer, M. Ibrahim, D. Tatro, F. Y. Feng, R. K. Ten Haken, A. Eisbruch, Mri to delineate the gross tumor volume of nasopharyngeal cancers: which sequences and planes should be used?, *Radiology and oncology* 48 (3) (2014) 323–330.

- [26] K.-L. Tseng, Y.-L. Lin, W. Hsu, C.-Y. Huang, Joint sequence learning and cross-modality convolution for 3d biomedical segmentation, in: Computer Vision and Pattern Recognition (CVPR), 2017 IEEE Conference on, IEEE, 2017, pp. 3739–3746.
- [27] C. Ma, G. Luo, K. Wang, Concatenated and connected random forests with multiscale patch driven active contour model for automated brain tumor segmentation of mr images, *IEEE Transactions on Medical Imaging*.
- [28] H. Cai, R. Verma, Y. Ou, S.-k. Lee, E. R. Melhem, C. Davatzikos, Probabilistic segmentation of brain tumors based on multi-modality magnetic resonance images, in: *Biomedical Imaging: From Nano to Macro, 2007. ISBI 2007. 4th IEEE International Symposium on*, IEEE, 2007, pp. 600–603.
- [29] B. H. Menze, A. Jakab, S. Bauer, J. Kalpathy-Cramer, K. Farahani, J. Kirby, Y. Burren, N. Porz, J. Slotboom, R. Wiest, et al., The multimodal brain tumor image segmentation benchmark (brats), *IEEE transactions on medical imaging* 34 (10) (2015) 1993.
- [30] G. E. Hinton, S. Osindero, Y.-W. Teh, A fast learning algorithm for deep belief nets, *Neural computation* 18 (7) (2006) 1527–1554.
- [31] K. Simonyan, A. Zisserman, Very deep convolutional networks for large-scale image recognition, *arXiv preprint arXiv:1409.1556*.
- [32] C. Szegedy, W. Liu, Y. Jia, P. Sermanet, S. Reed, D. Anguelov, D. Erhan, V. Vanhoucke, A. Rabinovich, Going deeper with convolutions, in: *Proceedings of the IEEE conference on computer vision and pattern recognition*, 2015, pp. 1–9.
- [33] K. He, X. Zhang, S. Ren, J. Sun, Deep residual learning for image recognition, in: *Proceedings of the IEEE conference on computer vision and pattern recognition*, 2016, pp. 770–778.

- [34] G. Huang, Z. Liu, L. Van Der Maaten, K. Q. Weinberger, Densely connected convolutional networks., in: CVPR, Vol. 1, 2017, p. 3.
- [35] J. Hu, L. Shen, G. Sun, Squeeze-and-excitation networks, arXiv preprint arXiv:1709.01507 7.
- [36] W. Liu, D. Anguelov, D. Erhan, C. Szegedy, S. Reed, C.-Y. Fu, A. C. Berg, Ssd: Single shot multibox detector, in: European conference on computer vision, Springer, 2016, pp. 21–37.
- [37] S. Ren, K. He, R. Girshick, J. Sun, Faster r-cnn: Towards real-time object detection with region proposal networks, in: Advances in neural information processing systems, 2015, pp. 91–99.
- [38] J. Redmon, A. Farhadi, Yolov3: An incremental improvement, arXiv preprint arXiv:1804.02767.
- [39] V. Badrinarayanan, A. Kendall, R. Cipolla, Segnet: A deep convolutional encoder-decoder architecture for image segmentation, IEEE Transactions on Pattern Analysis & Machine Intelligence (12) (2017) 2481–2495.
- [40] J. Long, E. Shelhamer, T. Darrell, Fully convolutional networks for semantic segmentation, in: Proceedings of the IEEE conference on computer vision and pattern recognition, 2015, pp. 3431–3440.
- [41] O. Ronneberger, P. Fischer, T. Brox, U-net: Convolutional networks for biomedical image segmentation, in: International Conference on Medical image computing and computer-assisted intervention, Springer, 2015, pp. 234–241.
- [42] L.-C. Chen, Y. Zhu, G. Papandreou, F. Schroff, H. Adam, Encoder-decoder with atrous separable convolution for semantic image segmentation, arXiv preprint arXiv:1802.02611.
- [43] M. Yang, K. Yu, C. Zhang, Z. Li, K. Yang, Denseaspp for semantic segmentation in street scenes, in: Proceedings of the IEEE Conference on Computer Vision and Pattern Recognition, 2018, pp. 3684–3692.

- [44] K. Kamnitsas, C. Ledig, V. F. Newcombe, J. P. Simpson, A. D. Kane, D. K. Menon, D. Rueckert, B. Glocker, Efficient multi-scale 3d cnn with fully connected crf for accurate brain lesion segmentation, *Medical image analysis* 36 (2017) 61–78.
- [45] Y.-J. Huang, Q. Dou, Z.-X. Wang, L.-Z. Liu, Y. Jin, C.-F. Li, L. Wang, H. Chen, R.-H. Xu, 3d roi-aware u-net for accurate and efficient colorectal tumor segmentation, *arXiv preprint arXiv:1806.10342*.
- [46] F. Milletari, N. Navab, S.-A. Ahmadi, V-net: Fully convolutional neural networks for volumetric medical image segmentation, in: *3D Vision (3DV), 2016 Fourth International Conference on*, IEEE, 2016, pp. 565–571.
- [47] V. V. Valindria, N. Pawlowski, M. Rajchl, I. Lavdas, E. O. Aboagye, A. G. Rockall, D. Rueckert, B. Glocker, Multi-modal learning from unpaired images: Application to multi-organ segmentation in ct and mri, in: *Applications of Computer Vision (WACV), 2018 IEEE Winter Conference on*, IEEE, 2018, pp. 547–556.
- [48] H. Zhao, J. Shi, X. Qi, X. Wang, J. Jia, Pyramid scene parsing network, in: *IEEE Conf. on Computer Vision and Pattern Recognition (CVPR)*, 2017, pp. 2881–2890.
- [49] L.-C. Chen, G. Papandreou, I. Kokkinos, K. Murphy, A. L. Yuille, Deeplab: Semantic image segmentation with deep convolutional nets, atrous convolution, and fully connected crfs, *IEEE transactions on pattern analysis and machine intelligence* 40 (4) (2018) 834–848.
- [50] H. Feldman, K. Friston, Attention, uncertainty, and free-energy, *Frontiers in human neuroscience* 4 (2010) 215.
- [51] L. Itti, C. Koch, E. Niebur, A model of saliency-based visual attention for rapid scene analysis, *IEEE Transactions on pattern analysis and machine intelligence* 20 (11) (1998) 1254–1259.

- [52] V. Mnih, N. Heess, A. Graves, et al., Recurrent models of visual attention, in: *Advances in neural information processing systems*, 2014, pp. 2204–2212.
- [53] F. Wang, M. Jiang, C. Qian, S. Yang, C. Li, H. Zhang, X. Wang, X. Tang, Residual attention network for image classification, in: *Proceedings of the IEEE Conference on Computer Vision and Pattern Recognition*, 2017, pp. 3156–3164.
- [54] S. Woo, J. Park, J.-Y. Lee, I. So Kweon, Cbam: Convolutional block attention module, in: *Proceedings of the European Conference on Computer Vision (ECCV)*, 2018, pp. 3–19.
- [55] K. Xu, J. Ba, R. Kiros, K. Cho, A. Courville, R. Salakhudinov, R. Zemel, Y. Bengio, Show, attend and tell: Neural image caption generation with visual attention, in: *International conference on machine learning*, 2015, pp. 2048–2057.
- [56] C. Cao, X. Liu, Y. Yang, Y. Yu, J. Wang, Z. Wang, Y. Huang, L. Wang, C. Huang, W. Xu, et al., Look and think twice: Capturing top-down visual attention with feedback convolutional neural networks, in: *Proceedings of the IEEE International Conference on Computer Vision*, 2015, pp. 2956–2964.
- [57] L. Chen, H. Zhang, J. Xiao, L. Nie, J. Shao, W. Liu, T.-S. Chua, Scann: Spatial and channel-wise attention in convolutional networks for image captioning, in: *2017 IEEE Conference on Computer Vision and Pattern Recognition (CVPR)*, IEEE, 2017, pp. 6298–6306.
- [58] A. Valada, R. Mohan, W. Burgard, Self-supervised model adaptation for multimodal semantic segmentation, *arXiv preprint arXiv:1808.03833*.
- [59] M.-x. Jiang, C. Deng, J.-s. Shan, Y.-y. Wang, Y.-j. Jia, X. Sun, Hierarchical multi-modal fusion fcn with attention model for rgb-d tracking, *Information Fusion* 50 (2019) 1–8.

- [60] M. Havaei, N. Guizard, N. Chapados, Y. Bengio, Hemis: Hetero-modal image segmentation, in: International Conference on Medical Image Computing and Computer-Assisted Intervention, Springer, 2016, pp. 469–477.
- [61] M. J. Jansen, H. J. Kuijf, J. P. Pluim, Automatic classification of focal liver lesions based on clinical dce-mr and t2-weighted images: A feasibility study, in: 2018 IEEE 15th International Symposium on Biomedical Imaging (ISBI 2018), IEEE, 2018, pp. 245–248.
- [62] X. Gao, W. Li, M. Loomes, L. Wang, A fused deep learning architecture for viewpoint classification of echocardiography, *Information Fusion* 36 (2017) 103–113.
- [63] Y. Liu, X. Chen, Z. Wang, Z. J. Wang, R. K. Ward, X. Wang, Deep learning for pixel-level image fusion: recent advances and future prospects, *Information Fusion* 42 (2018) 158–173.
- [64] A. P. James, B. V. Dasarathy, Medical image fusion: A survey of the state of the art, *Information Fusion* 19 (2014) 4–19.
- [65] Y. Liu, X. Chen, H. Peng, Z. Wang, Multi-focus image fusion with a deep convolutional neural network, *Information Fusion* 36 (2017) 191–207.
- [66] Y. Hu, M. Modat, E. Gibson, N. Ghavami, E. Bonmati, C. M. Moore, M. Emberton, J. A. Noble, D. C. Barratt, T. Vercauteren, Label-driven weakly-supervised learning for multimodal deformable image registration, in: Biomedical Imaging (ISBI 2018), 2018 IEEE 15th International Symposium on, IEEE, 2018, pp. 1070–1074.
- [67] B. Li, G. Yang, Z. Liu, J. L. Coatrieux, H. Shu, Multimodal medical image registration based on an information-theory measure with histogram estimation of continuous image representation, *Mathematical Problems in Engineering* 2018.

- [68] L. Zhang, Z. Liu, S. Zhang, X. Yang, H. Qiao, K. Huang, A. Hussain, Cross-modality interactive attention network for multispectral pedestrian detection, *Information Fusion* 50 (2019) 20–29.
- [69] W. Zhang, R. Li, H. Deng, L. Wang, W. Lin, S. Ji, D. Shen, Deep convolutional neural networks for multi-modality isointense infant brain image segmentation, *NeuroImage* 108 (2015) 214–224.
- [70] A. Valada, G. L. Oliveira, T. Brox, W. Burgard, Deep multispectral semantic scene understanding of forested environments using multimodal fusion, in: *International Symposium on Experimental Robotics*, Springer, 2016, pp. 465–477.
- [71] L. A. Gatys, A. S. Ecker, M. Bethge, Image style transfer using convolutional neural networks, in: *Proceedings of the IEEE Conference on Computer Vision and Pattern Recognition*, 2016, pp. 2414–2423.
- [72] C. Szegedy, V. Vanhoucke, S. Ioffe, J. Shlens, Z. Wojna, Rethinking the inception architecture for computer vision, in: *Proceedings of the IEEE conference on computer vision and pattern recognition*, 2016, pp. 2818–2826.
- [73] J. Yosinski, J. Clune, Y. Bengio, H. Lipson, How transferable are features in deep neural networks?, in: *Advances in neural information processing systems*, 2014, pp. 3320–3328.
- [74] N. Otsu, A threshold selection method from gray-level histograms, *IEEE transactions on systems, man, and cybernetics* 9 (1) (1979) 62–66.
- [75] D. P. Kingma, J. Ba, Adam: A method for stochastic optimization, *arXiv preprint arXiv:1412.6980*.